Lab on a Chip

Cite this: *Lab Chip*, 2012, **12**, 773

www.rsc.org/loc

PAPER

Uniform mixing in paper-based microfluidic systems using surface acoustic waves†

Amgad R. Rezk,[a] Aisha Qi,[a] James R. Friend,[a] Wai Ho Li[b] and Leslie Y. Yeo*[a]

Received 3rd November 2011, Accepted 12th December 2011
DOI: 10.1039/c2lc21065g

Paper-based microfluidics has recently received considerable interest due to their ease and low cost, making them extremely attractive as point-of-care diagnostic devices. The incorporation of basic fluid actuation and manipulation schemes on paper substrates, however, afford the possibility to extend the functionality of this simple technology to a much wider range of typical lab-on-a-chip operations, given its considerable advantages in terms of cost, size and integrability over conventional microfluidic substrates. We present a convective actuation mechanism in a simple paper-based microfluidic device using surface acoustic waves to drive mixing. Employing a Y-channel structure patterned onto paper, the mixing induced by the 30 MHz acoustic waves is shown to be consistent and rapid, overcoming several limitations associated with its capillary-driven passive mixing counterpart wherein irreproducibilities and nonuniformities are often encountered in the mixing along the channel—capillary-driven passive mixing offers only poor control, is strongly dependent on the paper's texture and fibre alignment, and permits backflow, all due to the scale of the fibres being significant in comparison to the length scales of the features in a microfluidic system. Using a novel hue-based colourimetric technique, the mixing speed and efficiency is compared between the two methods, and used to assess the effects of changing the input power, channel tortuousity and fibre/flow alignment for the acoustically-driven mixing. The hue-based technique offers several advantages over grayscale pixel intensity analysis techniques in facilitating quantification without limitations on the colour contrast of the samples, and can be used, for example, for quantification in on-chip immunochromatographic assays.

1 Introduction

The increasing costs of in-patient healthcare compounded by the chronic shortage of medical professionals in many developed nations underlie a need to shift diagnosis from the hospital to the patient at home or in the physician's office to facilitate prevention or early detection and timely treatment of disease. Widespread implementation of point-of-care testing, however, requires portable, inexpensive and reliable diagnostic technologies for which microfluidics has become a key area of research.[1] Nevertheless, few microfluidic diagnostic devices have been commercially successful, due to their complexity, difficulty in integration, and especially the cost of producing them in large quantities. Paper-based microfluidics offer an exciting alternative to standard polymer and integrated circuit substrate materials, potentially lowering the mass production costs of even complex microfluidics devices to serve the needs of healthcare systems in developed nations, and perhaps even to the point where the technology becomes an affordable solution to the unfortunate lack of even basic medical equipment or medical expertise in developing nations.[2,3]

In their simplest form, paper-based microfluidic diagnostics are based on lateral flow immunochromatographic assays (a well-known example being the home pregnancy test strip) where the physiological sample is drawn through a paper strip *via* capillary action to regions where antibodies specific to the detection protocol are immobilised. An absorbent pad placed at the waste end of the strip is often used to aid in drawing sufficient volume of the sample across the antibodies. Creative microfabrication and microfluidic strategies have recently been proposed to advance this simple technology beyond the one-dimensional lateral flow strip to allow for multiplex operation or multianalyte detection and to enhance detection sensitivity and quantification, whilst minimising the costs associated with producing these test kits.[4–9]

The ability to use paper in place of soft lithography polymer materials and especially silicon, glass and other such materials

[a]*Micro/Nanophysics Research Laboratory, School of Electrical & Computer Engineering, RMIT University, Melbourne, VIC, 3000, Australia. E-mail: leslie.yeo@rmit.edu.au*
[b]*Department of Electrical & Computer Systems Engineering, Monash University, Clayton, VIC, 3800, Australia*
† Electronic supplementary information (ESI) available. See DOI: 10.1039/c2lc21065g

typically employed for integrated circuit fabrication is justifiable on more than cost alone, given the convenience of working with it. Hydrodynamic focusing, dilution, mixing and separation schemes have been developed that employ capillary wetting, an attractively simple transport mechanism that eliminates the pumps and active mixing devices typical of standard microfluidics.[10]

Unfortunately, capillary wetting offers only rudimentary control over these processes. Moreover, irregularities in the porosity as well as the anisotropy, and, irregularity of the fibre orientation and length in paper altogether leads to nonuniformity and unpredictability in the capillary flow through the paper compared to flow in channels made from silicon, glass, or polymers in conventional microfluidic devices, especially for dynamic operation. When controllability and uniformity of the flow are important, an alternative to capillary flow is worth considering: active transport mechanisms through external forcing, *e.g.*, with electric or acoustic fields.[1,11] Whilst the introduction of such microfluidic actuation schemes appears contrary to the principle of simplicity and the inexpensive nature of paper-based devices, the advantages of controllability and uniformity help offset this concern, especially given recent developments in surface acoustic wave (SAW) microfluidic transport[12–14] that may be driven by inexpensive, miniature battery-powered circuits (see, for example, ref. 15) which can thus be integrated with the paper-based device.

In particular, SAWs have been shown to provide a useful means to extract bioanalyte molecules from paper substrates *via* atomisation for further analysis,[16] for example, using mass spectrometry.[17,18] Whilst this work focussed on the *post-atomisation* integrity of the molecular structures as they are transported through and *out* of the paper network,[16,18] we demonstrate here the possibility of extending the fast atomisation-induced fluid transport through paper to facilitate uniform mixing of two fluids *within* the paper structure, in particular, for the purpose of enabling low cost point-of-care paper-based diagnostics in a portable integrated device. Although the method is reminiscent of evaporative-driven transport inspired by transpiration in plants,[19] atomisation[20] does not rely on phase change, which is difficult to control and often requires stringent temperature regulation,[21] which can be costly and impractical in paper-based microfluidic devices. Moreover, the flow velocities generated using SAW atomisation, even in paper-based channels, are at least one to two orders of magnitude larger than the ultra-low flows in evaporative-driven transport in microfluidic channels or passive capillary-driven flows through paper channels. Further, the SAW mechanism is shown in this work to promote fast, uniform and consistent mixing in paper networks compared to that obtained *via* capillary action.

In quantifying the mixing performance, we introduce an alternative colourimetric technique employing the hue instead of the intensity (or brightness), enabling the use of multiple colours in a manner not possible with traditional methods that employ grayscale[22–24] or a specific colour channel, for example, the red component of the RGB colour space.[25] In addition, the method provides the ability to dynamically track the progression of the colour change both in space and time without requiring a large colour contrast as is required using grayscale analysis. Moreover, in contrast to grayscale methods which are based on intensity and hence sensitive to the illumination consistency across runs, the hue method is robust under different lighting conditions through normalisation by exploiting the property that hue values vary linearly with the colour scale. This also allows the method to easily be extended to include more than two colours. Finally, this quantitative technique can be employed to provide quantitative analysis and hence extend currently available immunochromatographic assays that are, at present, limited to visual qualitative tests,[26] such as the duplex test for influenza type A and type B antigens and triplex tests for HIV–1 and hepatitis B and C viruses.[27]

2. Materials and methods

2.1 Paper channels

Y-shaped flow channels with two inlets merged to form a single outlet channel were created in paper using a similar protocol to FLASH (Fast Lithographic Activation of Sheets).[28] The outlet channel was either patterned as a straight, curved in a serpentine fashion, or fabricated in a zigzag pattern with straight-line sections joined by sharp corners, as shown in Fig. 1. First, polyester-cellulose clean room paper (Lym-Tech, Chicopee, MA, USA) was soaked into a photoresist mixture (56.3% by volume SU8-25 + 37.5% by volume PGMEA + 6.2% by volume triarylsulfonium hexafluorophosphate salts (photoacid)) for 20–30 min to allow the paper to fully absorb the photoresist. After removing the paper from the solution and draining off excess photoresist, the paper was baked at 70 °C for several minutes

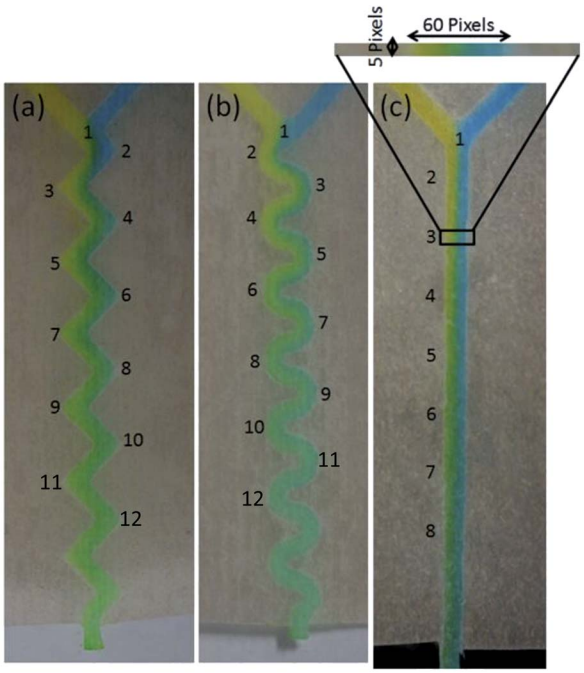

Location Number	1	2	3	4	5	6	7	8	9	10	11	12
Distance along the pathlength (mm)	0	4.55	9.1	13.65	18.2	22.75	27.3	31.85	36.4	40.95	45.5	50.05

Fig. 1 Different channel branch configurations and the mixing effect within: (a) zigzag, (b) curved, and (c) straight. The numeric labels indicate the locations at which the quantification is carried out.

until a semi-dry surface was obtained. The paper was then covered with an inexpensive polyester plastic film photomask for negative tone exposure (the channels were black at 4000 DPI resolution), exposed to UV flood lighting for 30 min and subsequently baked for 5–6 min until the surface became dry. The unexposed regions of the photoresist were then removed from the paper by immersing it in acetone for 1–2 min.

Although a variety of channel widths can be patterned, we demonstrate the technique with 2 mm wide channels. Narrower channels improve mixing, though at the cost of our ability to quantify the mixing—as the colour is assessed across the width of the channel in our structure that stretches over a length of 5 cm, even high resolution cameras are unable to accurately resolve the mixing with channels 1 mm in width or narrower whilst maintaining a field of view that encompasses the entire channel length. Though it is possible to zoom in to particular locations or use several cameras, the speed of the flow under certain conditions and the simple aim of the study in comparing behaviour between capillary- and SAW-driven mixing both suggest that, for now, a simple approach is best. Fluids were introduced onto the paper by first horizontally suspending two pipettes, each containing 10 $\mu\ell$ of coloured dye. To ensure that equivolumes of both fluids were deposited onto the paper at approximately the same time and location in both reservoirs, the pipette tips were then placed just above the paper surface and the plungers simultaneously pushed with equal displacements using a flat backing piece that spanned both plungers.

2.2 SAW device

Using standard UV lithography, chromium–aluminium elliptical SPUDT electrodes were patterned on a 127.86° $y-x$ rotated single crystal lithium niobate (LN) piezoelectric substrate (Fig. 2 (a)).[12] The gap and width of the interleaving electrode fingers were patterned to produce focused SAWs with 132 μm wavelengths, corresponding to a resonant frequency of 30 MHz. Applying a sinusoidal electrical signal at this frequency then generates a Rayleigh SAW propagating from the SPUDT towards a focal point on the substrate. The end of the paper channel is placed at this point (Fig. 2(b)). As depicted in Fig. 2(c), the fluid in the paper channel is drawn out to form a meniscus which subsequently atomises at the edge of the LN substrate, thereby resulting in a negative pressure gradient that draws fluid through the channel. For this method to work best in the paper microfluidics application, the channel structure must be pre-wetted. In the case of aqueous reagents, the channel can be pre-wetted using organic liquids given that these can still be atomised using the SAW.

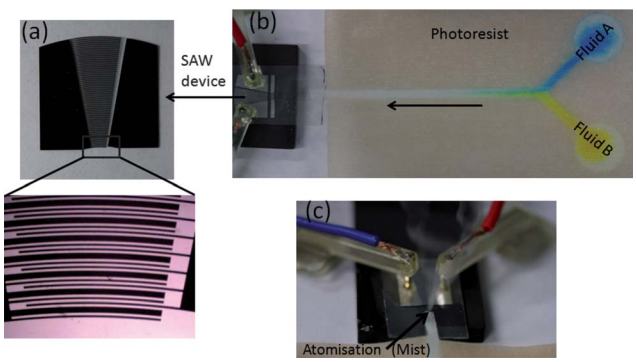

Fig. 2 (a) Image of the focused SPUDT across which an oscillating RF signal is applied to generate the SAWs that act to draw flow through the paper microfluidics device. (b) The end of the flow channel at the edge of the paper is placed at the focal point of the SAW such that (c) the atomisation of the fluid out of the channel at the paper edge draws liquid through the Y-channel from its two reservoirs.

2.3 Colourimetric analysis

Fluid mixing in microchannels is commonly quantified using grayscale techniques, either involving the standard deviation from a reference value or the mean value of the pixel intensity.[22,29] Both methods, however, require two fluids with a strong contrast in intensity between them—in other words, the grayscale technique works best when one fluid is bright and the other is dark in intensity in response to transmitted or reflected light. This often means that one fluid needs to be fluorescent and the other colourless to enable good quantification of their mixing. What this typically implies is that the analysis is not just limited to the mixing of two fluids—the limitation also extends to the type of fluids that can be used since a colour difference between the fluids alone is rarely sufficient for quantification. Moreover, such limitation in grayscale techniques also places severe restrictions on the quantification of immunochromatographic assays in practical diagnostic tests, and the detection of most colour *changes* in chemical reactions.

To the best of our knowledge, only one colourimetric technique has been proposed to date for quantifying the mixing intensity.[25] In this technique, the red component of the RGB colour space was used to quantify the mixing of a small quantity of red dye agitated in a transparent fluid container. As with grayscale models, this technique is limited to two fluids, one with a primary colour (red, green or blue) and the other colourless. Often, however, the analysis is restricted to the samples that are to be assessed and hence the choice of colour (or absence of colour, for that matter) is not always available, especially in practical diagnostic assays that may exhibit changes in colours over time or location without significant change in intensity.

To circumvent these limitations, we propose the *hue* as an independent means to quantify mixing. Every colour, independent of intensity (and hence the method and consistency of illumination), has a base hue value (see the colour bar in Fig. S1 in the ESI†). As the colour shade varies upon mixing, the hue values change correspondingly and can be tracked both spatially and temporally. For simplicity and to demonstrate the concept, we mix two aqueous solutions of different coloured food dyes from two separate reservoirs as they are drawn from the side Y-branches connecting the reservoirs into a single channel with the SAW. One reservoir contained a blue solution with hue $H_{\mathrm{blue}} \approx 210$ and the other contained a yellow solution with hue $H_{\mathrm{yellow}} \approx 50$, such that they form a green solution with a hue value $H_{\mathrm{green}} \approx 130$ when mixed in equal amounts and concentrations. More specifically, upon mixing two 10 $\mu\ell$ drops of the two coloured solutions, the hue changes to a value described fairly well by linear interpolation between the hues of the original solutions, using the ratio of the blue and yellow dye concentrations (Fig. S1 in the ESI†).

A digital SLR camera (EOS 550D, Canon, Utsnomiya, Japan) fitted with a macro lens (EF-S, 60 mm focal length, F/2.8, Canon, Utsnomiya, Japan) for high resolution imaging was used to photograph the fluid channel region in 0.5 s intervals, as shown in Fig. 1. Each image was processed to recover channel cross-sections 60 pixels wide by 5 pixels tall at specific locations along the channel's path length, taking into account their tortuousity. The hue values of the pixels were *normalised* as follows:

$$H_{\text{blue/yellow}} = \frac{H - H_{\text{green}}}{H_{\text{blue/yellow}} - H_{\text{green}}}; \quad (1)$$

a *mixing index* can then be obtained by averaging this normalised hue value over the 300 pixels in each channel cross-section at steady-state. Each run was performed three times to assess the variability in the results; the reported data is thus the statistical result of all three runs. Due to the way the normalisation is performed, either unmixed blue or yellow will give a normalised hue value of 1, while a fully mixed combination of equal parts of blue and yellow to give green will result in a normalised hue value of 0. For each of the positions along the microfluidic path, the average normalised hue value can also be determined as a function of time—this is shown in Fig. S2 in the ESI† for the curved channel in Fig. 1(b).

3 Results and discussion

3.1 SAW-driven flow compared to capillary-driven flow

Fig. 3 shows a comparison between the wetting speeds due to pure capillary action in which fluid is *pushed* through the channel and that due to the SAW in which fluid is *pulled* through the channel. It is clear that the mechanism by which fluid is transported along the paper channel using SAW is somewhat different to capillary imbibition through the paper pores, predicted by the Washburn scaling $x \sim t^{1/2}$ (x being the length along the channel traversed by the advancing fluid front and t being time)[30–32] that arises from a balance between the viscous and capillary stresses

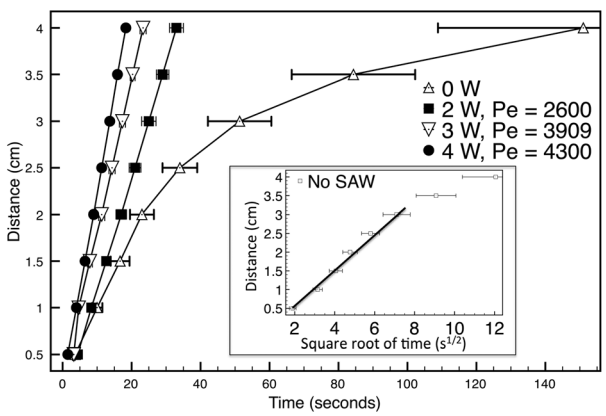

Fig. 3 A comparison of the wetting speed through the paper channel for capillary- and SAW-driven transport (with various input power levels) indicates the nearly constant velocity flow induced by the SAW and the recovery of the Washburn model prediction for capillary-driven fluid transport. The former is substantially faster for channels longer than about 2 cm. The inset shows a rescaling of the data for the capillary-driven flow (0 W), indicating that the flow eventually slows beyond the predicted rate of the Washburn model due to evaporation.

that dominate the flow behaviour. Over longer periods of time, evaporation causes the flow to deviate from the Washburn model, as shown in the inset of Fig. 3—such behaviour was also observed elsewhere.[33] In contrast, the negative pressure gradient generated within the paper channel due to the SAW atomisation at the edge of the channel drives flow within the channel which can be characterised by a balance between the dynamic pressure and capillary stress, yielding $x \sim t$ in agreement with the linear response exhibited in Fig. 3. This indicates a dominant convective mechanism in which fluid is transported *over* the paper surface rather than *through* the pores of the paper.

The SAW-driven convective transport of the fluid over the paper nevertheless provides more than merely higher flow speeds (and hence reduced assay times, thereby reducing problems due to evaporation and dryout in paper-based assays). The SAW-driven flow is observed to be more uniform and predictable compared to its capillary-driven counterpart, in which inconsistencies in the flow behaviour are commonly observed due to irregularities in the fibre alignment and length—the source of the large error bars in Fig. 3 and the poor behaviour observed in the mixing experiments we describe below (see, for example, Fig. 4 (a))—this despite the higher quality and more expensive clean room paper used in this study. Even if the fibre orientation could be controlled, the scale of the fibres is significant in comparison to most *micro*fluidic structures, and anisotropy exists in the wetting characteristics between the direction along the fibres to across them, both of which also lead to irregularity in the flow.

Another advantage of SAW transport is the elimination of backflow, where capillary flow from one inlet reservoir travels down to the Y-junction and both down the outlet leg as well as up the inlet leg of the other reservoir (Fig. 4(b)). This can occur if a fluid is not present at the Y-junction or if there is an imbalance between the capillary pressures of the two fluids. Such backflows can significantly affect the downstream channel behaviour (and hence the mixing in the experiments to be described subsequently), where one fluid reaches the junction before the other, causing a partial blockage in which the section of the channel available for the second fluid to flow is reduced (Fig. 4(a)). Backflow can also lead to wastage, which is a concern if expensive reagents or samples are involved.

3.2 Mixing performance

These undesirable effects in capillary-driven flow translate to irregularities when mixing is attempted in paper microfluidics. The image at 40 s in Fig. 4(a) illustrates the effect of one Y-branch of the channel being partially blocked by fluid from the other Y-branch due to backflow as a consequence of an imbalance of the capillary pressure between both reservoirs (we note that this effect appears to be random and cannot be attributed to the faster mobility of, in this case, the blue dye in the paper over the yellow dye—reversing the dyes resulted in equally random behaviour, which arises due to the irregularities in the paper structure). We observe not only the advancing front to be irregular but also the mixing to be erratic and nonuniform along the channel length. Good mixing is observed to appear, for example, at the junction where the branches intersect followed by poorer mixing downstream in the straight channel. The mixing performance thereafter recovers at some downstream location

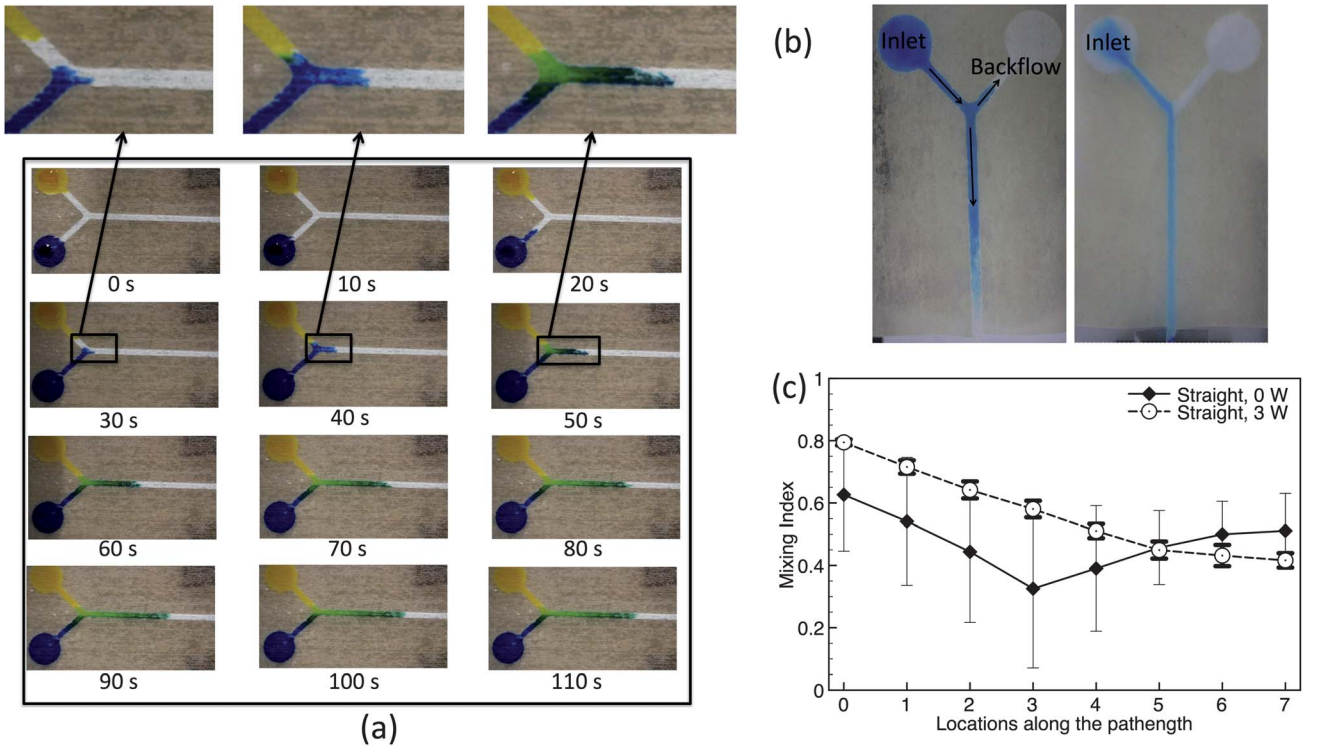

Fig. 4 (a) Time series of images showing the mixing of two coloured solutions in a straight Y-channel (Fig. 1(c)) when driven by pure capillary wetting through the paper. The enlarged images above show an example of backflow of one solution from one Y-branch into another due to the imbalance of capillary pressures between the two reservoirs. As a consequence, the capillary wetting front suffers from irregularities and the subsequent mixing appears to be nonuniform. Good mixing is observed at the Y-junction but deteriorates downstream due to wetting irregularities and blockages in the flow. The mixing index in panel (c) quantifies this behaviour. (b) Capillary-driven fluid transport showing backflow arising when a fluid is placed in one inlet (left), while transport using the SAW pulls the fluid from the inlet towards the outlet without backflow (right). It is worthwhile noting that three times as much volume of the sample fluid had to be placed in the capillary-driven system to fill the identically sized channel to the same extent. (c) Comparison of the mixing performance between capillary and SAW-driven flows in the straight channel. The large error bars for capillary-driven mixing arise due to poor repeatability, a consequence of the paper's nonuniformity.

only to deteriorate once again. The mixing nonuniformity can be more clearly seen in the large error bars as well as the dip (location 4) and subsequent rise in the mixing index associated with the data for capillary-driven mixing (0 W) in Fig. 4(c). The large variation in the data arises as a consequence of inconsistent runs. In comparison, the mixing in the same straight channel (Fig. 1(c)) generated by the SAW appears to be considerably more uniform, with little variation in the mixing intensity for each of the measured locations from run to run. Such repeatability in the results can often be an important consideration in practical diagnostic devices, especially for quantitative tests, and hence the advantage of using the SAW to achieve such repeatability could in these circumstances outweigh the cost of the inclusion of an active transport mechanism.

In addition to more uniform and predictable mixing, we also note enhancement in the mixing performance. This can be seen more evidently by comparing the transverse concentration profile across the paper channel with that predicted by a steady convective-diffusive model, which, in dimensionless form, reads

$$\mathrm{Pe}\frac{\partial c^*}{\partial x^*} = \frac{\partial^2 c^*}{\partial x^{*2}} + \frac{\partial^2 c^*}{\partial y^{*2}}, \qquad (2)$$

wherein the asterisks (*) denote dimensionless quantities: the axial and transverse coordinates are scaled with the channel width, *i.e.*, $(x^*,y^*) \equiv (x,y)/W$, and the concentration is scaled with the initial concentration, *i.e.*, $c^* \equiv c/c_o$. In this case, we take c to be the concentration of the blue dye; c_o is hence the concentration in the reservoir. $\mathrm{Pe} \equiv UW/D$ is the Péclet number, which captures the relative contributions between convective and diffusive transport. D is the diffusivity and U is the average velocity at which the SAW pulls the fluid through the channel, which, from Fig. 3 can be assumed constant; from our experimental observations, it is also not unreasonable to assume that U is uniform across the channel cross-section. At the inlet of the straight channel $x^* = 0$, the initial unmixed condition requires $c^* = 1$ for $0 \le y^* < 0.5$ and $c^* = 0$ for $0.5 \le y^* \le 1$, whereas a no-flux condition $\partial c^*/\partial x^* = 0$ can be imposed at the outlet ($x^* \to \infty$, $0 \le y^* \le 1$). Further, we assume that the channel sidewalls are impermeable, *i.e.*, $\partial c^*/\partial y^* = 0$ at $y^* = 0,1$ for all x^*. Eqn (2), subject to these boundary conditions, has an analytical solution of the form[34]

$$c^*(x^*,y^*) = 0.5 + \frac{2}{\pi}\sum_{n=1}^{\infty}\frac{\sin(n\pi/2)}{n}\cos(n\pi y^*)$$

$$\exp\left(-\frac{2n^2\pi^2 x^*}{\mathrm{Pe}+\sqrt{\mathrm{Pe}^2+4n^2\pi^2}}\right). \qquad (3)$$

Fig. S3 in the ESI† shows the concentration profile predicted by eqn (3) and that obtained from the experiment for an input

power of 2 W, which given $U = 1.33 \times 10^{-3}$ m s^{-1}, $W = 2$ mm and $D_o = 10^{-9}$ m^2 s^{-1}, corresponds to Pe = 2600, at a representative location along the channel length; here, we take the position roughly corresponding to the middle of the channel length, $x^* = 10$. It can be seen that the theory considerably underpredicts the mixing compared to the experimental profile at the same location. It is nevertheless possible to capture, at least approximately, the mixing enhancement of the SAW-driven transport above that given by the standard convective-diffusive model using an effective diffusivity, D_{eff}—we observe that the analytical and experimental concentration profiles appear to roughly match when $D_{\text{eff}} = 10D_o$, corresponding to a tenfold decrease in the Péclet number ($\text{Pe}_{\text{eff}} = 260$).

Whilst the similar exponential trends for the analytical and experimental transverse concentration profiles indicate that the mixing in the paper channels indeed occurs *via* diffusion between the laminar streams, we note that the mixing enhancement does not arise directly due to the SAW-driven convective transport along the channel (Section 3.1). In contrast to fast and chaotic mixing driven by SAW convection in a *sessile drop*,[35–39] we observe little effect of increasing the input power to the SAW (corresponding to an increase in the speed at which fluid is transported along the paper channel (Fig. 3) and hence the Péclet number) on the mixing performance, as seen in Fig. 5(a). This is confirmed by the analytical prediction in Fig. S3 in the ESI,† which shows little change in the concentration profiles, for an increase in the effective Péclet number from 260 to 430 to account for the higher flow velocity as the power is increased. In fact, the faster flow leads to a slight deterioration in the mixing performance due to the reduced residence time of the fluid in the paper. The mixing enhancement also cannot be due to increased interfacial area of contact for mixing as no significant changes to the interface between the two parallel laminar streams was observed.

Another mechanism must therefore be responsible for the mixing enhancement captured through the effective diffusivity above: the obstruction to the flow posed by the paper fibres over which the fluid has to be transported—a paper analogue of the flow structures patterned in microchannels (*e.g.*, grooves,[23] slants[40] or obstacles[41]) designed to break the laminarity of the flow. This mechanism becomes clearly evident when we deliberately drive the flow at an angle to the fibre orientation (see inset of Fig. 5(a)) wherein the misalignment between the channel (and hence flow direction) and the fibre orientation is observed to lead to further improvement in the mixing performance, as seen in Fig. 5(a). This is in sharp contrast to capillary-driven flow where the fibre orientation actually governs the direction in which the fluid is transported, and random fibre misalignment often leads to irregularities in both the flow speed and mixing behaviour.

It is possible to further enhance the mixing improvement due to the presence of the fibres by increasing or spatially-varying the flow/fibre misalignment by introducing tortuousity in the channel. To illustrate this, we patterned both zigzag and curved channels, as shown in Fig. 1(a) and Figs. 1(b), in which we observe considerable improvement in the mixing performance (Fig. 5(b)). It should be noted that the mixing enhancement cannot not attributed to the vortical structures induced by Dean flows that was previously shown in curved microchannels.[42] Given a channel hydraulic diameter $D_{\text{H}} \approx 0.002$ mm, radius of curvature of the flow path $R \approx 3$ mm, and Reynolds number $\text{Re} \equiv \rho UW/\mu \sim O(1)$ (ρ and μ being the fluid density and viscosity), the Dean number $\kappa \equiv \left(\sqrt{D_{\text{H}}/2R}\right)\text{Re} \sim O(0.01)$ is small. This suggests that the Dean flow due to the channel curvature is weak and any mixing enhancement arising from flow vorticity can be neglected. In contrast, the mixing enhancement due to the channel tortuousity can be attributed to the amplification of the flow/fibre misalignment effect as the flow is forced to traverse the fibres multiple times as it is guided through the tortuous channel geometry. Handedness effects in the mixing are apparent though, arising from the asymmetry in the outlet channel from the Y-junction. For example, as seen in Fig. 1 as well as Fig. 5(b), there is poorer mixing on the right-hand bends at the odd-numbered locations (3, 5, 7 and 9) compared to the left-hand bends at the even-numbered locations (2, 4, 6, 8 and 10) for the zigzag and curved channels. The handedness is however more prominent in the zigzag channels due to the sharp bends.

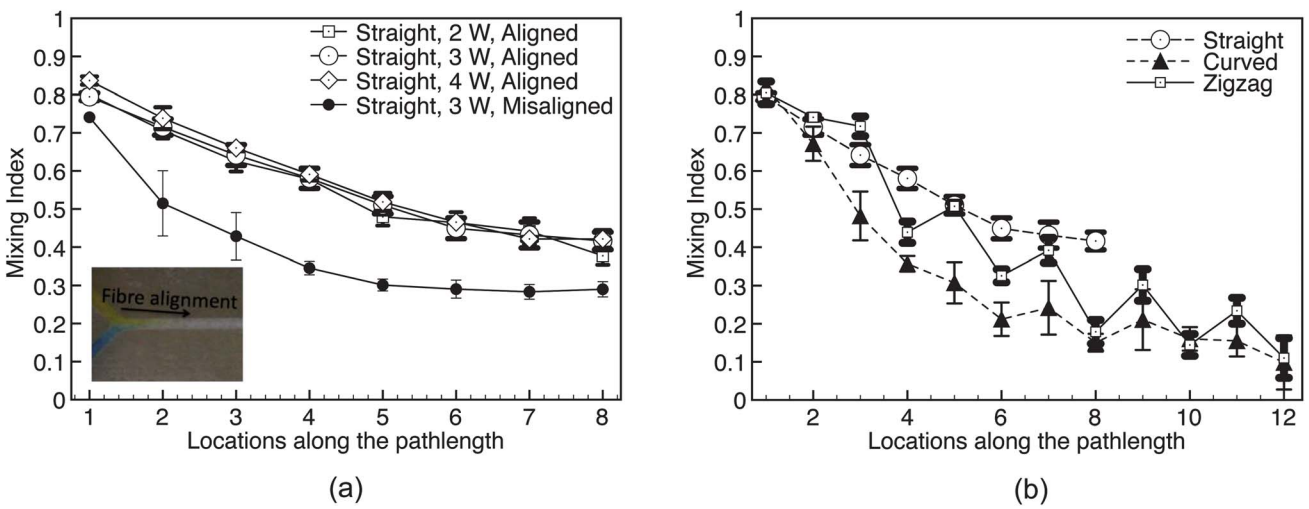

Fig. 5 (a) Effect of the input power and flow/fibre alignment on mixing performance. The inset shows the direction of the flow with respect to the fibre orientation. (b) Comparison of the mixing performance between the straight, curved and zigzag channels shown in Fig. 1. The straight channel gave the poorest mixing performance, taking into account the different path lengths, whilst the curved channel provides the best mixing, albeit with some minor handedness effects due to the asymmetry of the junction where the Y-branches intersect.

4 Conclusions

Paper-based microfluidic systems offer a simple, low-cost and disposable alternative for point-of-care diagnostics. Whilst the single-strip lateral flow immunochromatographic assay is now used for a wide range of diagnostic testing, advances in paper microfluidic networks offer significant opportunity in applications beyond simple qualitative tests to multiplex, sensitive and quantitative assays not only for third-world diagnostics but also for field-use environmental monitoring, smart food labelling and drug development, amongst other applications. The obvious advantages of these paper-based systems over conventional microfluidic substrates also provide justification to broaden their functionality to replicate that of the silicon and PDMS counterparts. This, however, requires typical microfluidic operations such as flow actuation and bioparticle manipulation to be carried out on paper substrates. Here, we demonstrate the use of SAWs, powerful fluid actuation and manipulation tools already part of the microfluidic arsenal, to drive the flow and induce uniform mixing in paper-based microfluidic channels. Though at the expense of introducing external forcing, we show that nonuniformities and poor reproducibility in passive mixing in paper networks that arise as a consequence of limitations unique to capillary-driven flow in paper can be circumvented to provide faster, more uniform, repeatable and predictable mixing on paper. The expense in terms of cost, size and integrability is however minimal with SAW actuation since it has been previously shown that the highly efficient fluid-mechanical coupling allows a wide range of microfluidic operations to be carried out in an inexpensive chip-sized device at very low powers driven by a miniature battery-powered circuit that can easily be integrated. In the process of examining various parameters that control the flow speed and mixing efficiency, such as input power, channel shape/tortousity and fibre/flow alignment, we also introduce a new hue-based colourimetric technique that allows for mixing quantification without limitations on the colour and contrast of the samples.

Acknowledgements

The authors thank Darren Kamil for his help with the initial feasibility experiments as well as Xiaofei Shi for her help with the development of the colourimetric technique. This work is funded through an Australian Research Council Discovery Grant DP0985266, through which LYY grateful acknowledges support for an Australian Research Fellowship.

References

1 L. Y. Yeo, H.-C. Chang, P. P. Y. Chan and J. R. Friend, *Small*, 2011, **7**, 12–48.
2 P. Yager, T. Edwards, E. Fu, K. Helton, K. Nelson, M. R. Tam and B. H. Weigl, *Nature*, 2006, **442**, 412–418.
3 A. W. Martinez, S. T. Phillips, G. M. Whitesides and E. Carrilho, *Anal. Chem.*, 2010, **82**, 3–10.
4 A. W. Martinez, S. T. Phillips and G. M. Whitesides, *Proc. Natl. Acad. Sci. U. S. A.*, 2008, **105**, 19606–19611.
5 K. Abe, K. Suzuki and D. Citterio, *Anal. Chem.*, 2008, **80**, 6928–6934.
6 A. Martinez, S. Phillips, M. Butte and G. Whitesides, *Angew. Chem., Int. Ed.*, 2007, **46**, 1318–1320.
7 E. M. Fenton, M. R. Mascarenas, G. P. Lopez and S. S. Sibbett, *ACS Appl. Mater. Interfaces*, 2009, **1**, 124–129.
8 E. Fu, P. Kauffman, B. Lutz and P. Yager, *Sens. Actuators, B*, 2010, **149**, 325–328.
9 E. Fu, B. Lutz, P. Kauffman and P. Yager, *Lab Chip*, 2010, **10**, 918–920.
10 J. L. Osborn, B. Lutz, E. Fu, P. Kauffman, D. Y. Stevens and P. Yager, *Lab Chip*, 2010, **10**, 2659–2665.
11 H. Stone, A. Stroock and A. Ajdari, *Annu. Rev. Fluid Mech.*, 2004, **36**, 381–411.
12 L. Y. Yeo and J. R. Friend, *Biomicrofluidics*, 2009, **3**, 012002.
13 J. Friend and L. Y. Yeo, *Rev. Mod. Phys.*, 2011, **83**, 647–704.
14 Z. Wang and J. Zhe, *Lab Chip*, 2011, **11**, 1280–1285.
15 A. Qi, J. R. Friend, L. Y. Yeo, D. A. V. Morton, M. P. McIntosh and L. Spiccia, *Lab Chip*, 2009, **9**, 2184–2193.
16 A. Qi, L. Yeo, J. Friend and J. Ho, *Lab Chip*, 2010, **10**, 470–476.
17 S. R. Heron, R. Wilson, S. A. Shaffer, D. R. Goodlett and J. M. Cooper, *Anal. Chem.*, 2010, **82**, 3985–3989.
18 J. Ho, M. K. Tan, D. B. Go, L. Y. Yeo, J. R. Friend and H.-C. Chang, *Analytical Chemistry*, 2011, **83**, 3260–3266.
19 V. Namasivayam, R. G. Larson, D. T. Burke and M. A. Burns, *J. Micromech. Microeng.*, 2003, **13**, 261–271.
20 A. Qi, L. Y. Yeo and J. R. Friend, *Phys. Fluids*, 2008, **20**, 074103.
21 M. Zimmermann, S. Bentley, H. Schmid, P. Hunziker and E. Delamarche, *Lab Chip*, 2005, **5**, 1355–1359.
22 R. H. Liu, M. A. Stremler, K. V. Sharp, M. G. Olsen, J. G. Santiago, R. J. Adrian, H. Aref and D. J. Beebe, *J. Microelectromech. Syst.*, 2000, **9**, 190–197.
23 A. D. Stroock, S. K. W. Dertinger, A. Ajdari, I. Mezić, H. A. Stone and G. M. Whitesides, *Science*, 2002, **295**, 647–651.
24 J.-H. Kim, B.-G. Kim, H. Nam, D.-E. Park, K.-S. Yun, J.-B. Yoon, J. You and E. Yoon, *Proceedings of the Fifteenth IEEE International Conference on Micro Electro Mechanical Systems*, 2002, 133–136.
25 F. Cabaret, S. Bonnot, L. Fradette and P. A. Tanguy, *Ind. Eng. Chem. Res.*, 2007, **46**, 5032–5042.
26 P. J. Mazzone, J. Hammel, R. Dweik, J. Na, C. Czich, D. Laskowski and T. Mekhail, *Thorax*, 2007, **62**, 565–568.
27 M. A. Dineva, D. Candotti, F. Fletcher-Brown, J.-P. Allain and H. Lee, *J. Clin. Microbiol.*, 2005, **43**, 4015–4021.
28 A. W. Martinez, S. T. Phillips, B. J. Wiley, M. Gupta and G. M. Whitesides, *Lab Chip*, 2008, **8**, 2146–2150.
29 N.-T. Nguyen and Z. Wu, *J. Micromech. Microeng.*, 2005, **15**, R1–R16.
30 E. W. Washburn, *Phys. Rev.*, 1921, **17**, 273–283.
31 R. L. Peek and D. A. McLean, *Ind. Eng. Chem., Anal. Ed.*, 1934, **6**, 85–90.
32 E. Fu, S. Ramsey, P. Kauffman, B. Lutz and P. Yager, *Microfluid. Nanofluid.*, 2011, **10**, 29–35.
33 D. R. Ballerini, X. Li and W. Shen, *Biomicrofluidics*, 2011, **5**, 014105.
34 Z. Wu and N.-T. Nguyen, *Microfluid. Nanofluid.*, 2005, **1**, 208–217.
35 H. Li, J. Friend and L. Yeo, *Biomed. Microdevices*, 2007, **9**, 647–656.
36 R. Shilton, M. K. Tan, L. Y. Yeo and J. R. Friend, *J. Appl. Phys.*, 2008, **104**, 014910.
37 T. Frommelt, M. Kostur, M. Wenzel-Schäfer, P. Talkner, P. Hänggi and A. Wixforth, *Phys. Rev. Lett.*, 2008, **100**, 034502.
38 T.-D. Luong, V.-N. Phan and N.-T. Nguyen, *Microfluid. Nanofluid.*, 2011, **10**, 619–625.
39 R. Shilton, J. R. Friend and L. Y. Yeo, *Sens. Actuators, B*, 2011, **160**, 1565–1572.
40 T. J. Johnson, D. Ross and L. E. Locascio, *Anal. Chem.*, 2001, **74**, 45–51.
41 H. Wang, P. Iovenitti, E. Harvey and S. Masood, *Smart Mater. Struct.*, 2002, **11**, 662–667.
42 A. Sudarsan and V. Ugaz, *Proc. Natl. Acad. Sci. U. S. A.*, 2006, **103**, 7228–7233.